https://doi.org/10.5194/gmd-2023-94
Preprint. Discussion started: 18 August 2023

Geoscientific Model Development Discussions

Three-Dimensional Analytical Solution of Self-potential from Regularly Polarized Bodies in Layered Seafloor Model

Pengfei Zhang[1 2 3], Yi-an Cui[1 2 3], Jing Xie[1 2 3], Youjun Guo[1 2 3], Jianxin Liu[1 2 3], and Jieran Liu[1 2 3]

[1]School of Geosciences and Info-Physics, Central South University, Changsha, 410083, China
[2]Laboratory of Non-ferrous Resources and Geological Hazard Detection, Central South University, Changsha, 410083, China
[3]Key Laboratory of Metallogenic Prediction of Nonferrous Metals, Ministry of Education, Central South University, Changsha, 410083, China

Correspondence: Yi-an Cui (cuiyian@csu.edu.cn)

Abstract. The self-potential (SP) method is a sensitive geophysical means to locate seafloor polymetallic sulfide deposits. A reasonable SP forward modeling can provide a good foundation for inversion and interpretation of the measured data. We propose a method to solve the analytical solution of the SP generated by regularly polarized bodies in layered media. Based on the mirror image current theory, a new analytical formula was derived and clarified in detail for the models. We also discussed the analytical solution of layered models with different numbers of layers through numerical computation. Furthermore, a lab-based oxidation-reduction experiment was conducted to record the SP data. These data were used to simulate the SP generated by seafloor massive sulfide(SMS) deposits and assess the analytical solution previously. The result shows that the measured SP data matches the analytical solution well. That demonstrates the correctness of the proposed method and the corresponding analytical solution. It is significant to fast and precise forward modeling and inversion for SMS explorations.

1 Introduction

Seafloor massive sulfide(SMS) deposit is an important strategic resource for its rich gold, silver, copper, zinc, and other high-value metal ore (Mendonca, 2008). The research of submarine hydrothermal vents at the Galapagos in 1977 is the beginning of the seafloor massive sulfide which continues today (Corliss et al., 1979). More than 700 submarine hydrothermal anomalies have been discovered. And there are more than 100 areas with exploration potential up to now (Hannington et al., 2011). The self-potential method is a passive source method and needs no power source during nature conditions (Guo et al., 2022; Fornasari et al.). The seafloor is a special redox interface. Electrical conductors formed by mineral deposits will generate an electric current when they cross this interface. The SP survey has a unique response to this abnormal electric current and can locate the SMS deposits quickly. Corwin was the first to attempt to measure the SP signal in marine minerals with an offshore SP array and recorded an abnormal signal of up to 300 mV (Corwin, 1976).For instance, Safipour et al. recorded both horizontal components of a known site containing an SMS occurrence and proved that the SP method is an effective exploration tool in SMS areas with hydrothermal activity (Safipour et al., 2017).Kawada and Constable observed SP signals of SMS with a deep-tow handled an AUV respectively, which further proved the SP method is useful in SMS exploration (Kawada and Kasaya, 2017; Constable et al., 2018). Su et al. used an autonomous underwater vehicle to take a SP survey on the ultraslow-spreading

https://doi.org/10.5194/gmd-2023-94
Preprint. Discussion started: 18 August 2023


Geoscientific Model Development Discussions

Southwest Indian Ridge with a water depth from 1300m to 2200m. And a 3D SP tomography was used to reveal an ore-body with a vertical extent of 100m (Su et al., 2022). The above researches suggest that the self-potential method contributes to seafloor massive sulfide surveys.

The forward methods commonly used for self-potential methods include numerical solutions and analytical solutions. The numerical solution is a qualitative (or semi-quantitative) technique (Wei et al., 2023), which includes the finite element method (Alarouj and Jackson, 2022; Bérubé, 2007), the finite volume method (Sheffer and Oldenburg, 2007), the finite difference method (Xie et al., 2020a), the natural-infinite element coupling method (Xie et al., 2020b), the finite-infinite element coupling method (Xie et al., 2020c)and so on. Numerical modeling applies to any complex model. Xie et al. proposed a finite-infinite element coupling method to calculate a 3-D numerical model of the marine SP from seafloor hydrothermal sulfide deposits (Xie et al., 2021b).However, the result of numerical method is obtained by approximate calculation under a certain condition. The solution of the stiffness matrix is complicated because of the affection of the field source. Take a sphere as an example, the polarization intensity of its surface does not vary uniformly. And for the numerical method, the complex artificial boundary conditions also limit its development. Compared with the numerical method, the analytical solutions are strict formulas which occur difficulty in solving the Poisson equation. In most studies, the polarization structure of ore bodies can be equivalent to special geometry shapes. The analytical solution of polarized geometry body is significant in mineral exploration. Yungul discussed the analytical solution of a polarized sphere and other researchers get the analytical solution of SP anomaly along a profile passing over the centre of the sphere or to the strike of a horizontal cylinder (Yungul, 1950; Bhattacharya and Roy, 1981; El-Araby, 2004). Murthy and Haricharan discussed the analytical solution of SP anomaly at any point on a profile perpendicular to the strike of a 2-D inclined thin sheet (Satyanarayana Murty and Haricharan, 1985). Further, Biswas derived the expression of SP anomaly analytical solution when the sheet parameters were described with respect to one edge of the sheet and in terms of the **X** and **Z** coordinate of the top and bottom edge of the sheet(Biswas and Sharma, 2014). Dmitriev derived the analytical solution of SP anomaly at point **M** on the surface due to a thick dipping body which could represent an ore body(Dmitriev, 2012).The above analytical solutions are 2D. In marine fieldwork, it's difficult to locate the centre or the strike of different geometric bodies. We proposed a 3D analytical solution based on the mirror image method for layered SMS model.

2 The mirror image method of electric dipole

The mirror image method is based on the uniqueness theorem. It can be used to solve the electrostatic field problem such as some special problems of conductor boundary with point source or line source(Stephenson, 1990). The uniqueness theorem states that there is only one solution in the electrostatic system when the boundary conditions are uniquely determined(Wang et al., 2019). A SMS model which meets the uniqueness theorem is built as shown in Fig.1. **XOY** surface is the boundary between the sea and the air. We suppose the depth of seawater is D and the depth of the seafloor is L. A three-dimensional coordinate system is established with vertical sea level downward as the Z-axis. We use ε,μ, σ to denote the medium permittivity, magnetic conductivity and conductivity and use subscripts 0,1,2 to denote air, seawater and seafloor. We suppose there

https://doi.org/10.5194/gmd-2023-94
Preprint. Discussion started: 18 August 2023

Geoscientific Model Development Discussions

is an electric dipole $P = \mathbf{I}d\mathbf{l}$ in any direction located at (x_0, y_0, z_0), z_0<D and the measuring point is at (x, y, z). If $z \leq 0$, the measuring point is in the air or on the sea surface.If $0 <$z$< H$, the measuring point is in seawater. The horizontal electric dipole is parallel to the plane z=0 and the vertical electric dipole is parallel to the z-axis. The following derivation process is based on the example of a horizontal electric dipole $P_x = \mathbf{I}_x d\mathbf{l}i$.

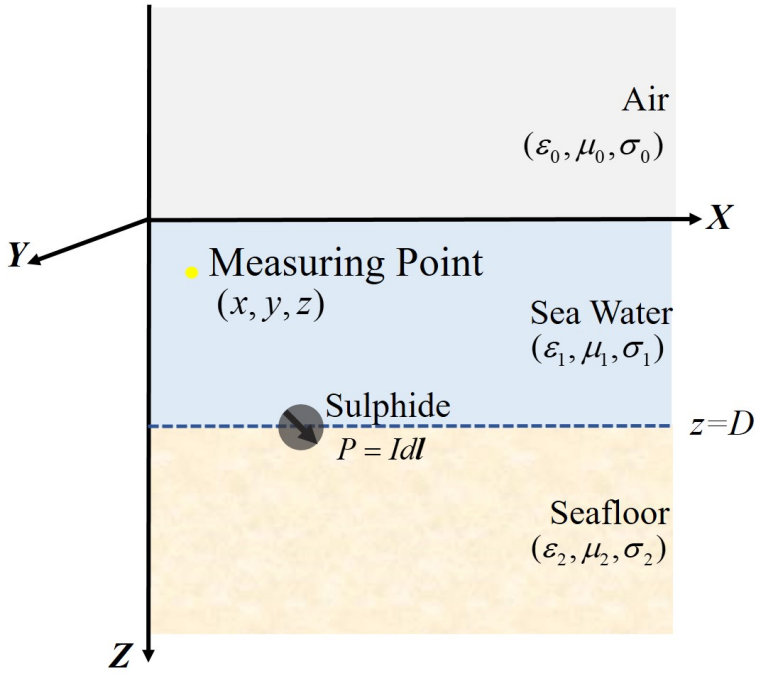

Figure 1. Sketch of SMS simplified model. The model includes air, seawater and seafloor. The Z axis points down towards the seafloor.

2.1 Potential equivalence of the sphere and the electric dipole

An uneven double electric layer forms on the surface of the polarized sphere. The potential difference $\Delta\varepsilon$ varies linearly with the direction of polarization, which can be expressed as

$$\Delta\varepsilon=\Delta U_0 \cos\theta \tag{1}$$

where ΔU_0 is the maximum potential difference. θ is the angle between the polarization axis and the line from the measuring point to the sphere centre. This formula accords with the Laplace equation in spherical coordinates:

$$\frac{\partial}{\partial R}(R^2\frac{\partial U}{\partial r}) + \frac{1}{\sin\theta}\cdot\frac{\partial}{\partial\theta}(\sin\theta\frac{\partial U}{\partial\theta}) = 0 \tag{2}$$

The general solution of potential can be solved as

$$U=\sum_{n=0}^{\infty}(A_n R^n + B_n/R^{n+1})P_n(\cos\theta) \tag{3}$$

https://doi.org/10.5194/gmd-2023-94
Preprint. Discussion started: 18 August 2023

Geoscientific Model Development Discussions
Open Access
EGU

Where $P_n(cos\theta)$ is Legendre polynomial of n, An and Bn is undetermined coefficient. Based on the boundary conditions:

1) There is a potential jump on both sides of the sphere. When $R = r0$, we have:

$$\Delta\varepsilon{=}U_2 - U_1 = \Delta U_0 \cos\theta \tag{4}$$

Where U_1 and U_2 is the potential outside and inside the sphere.

2) The current density normal vectors are continuous on both sides of the sphere. When $R = r0$ we have:

$$\frac{1}{\rho_1}\frac{\partial U_1}{\partial R}{=}\frac{1}{\rho_2}\frac{\partial U_2}{\partial R} \tag{5}$$

The sulfide potential anomaly caused by a sphere is obtained by the formula(Li et al., 2005)

$$U = M\frac{\cos\theta}{r^2}, M = \frac{2\rho_1}{2\rho_2 + \rho_1}r_0^2\Delta U_0 \tag{6}$$

Where θ is the polarization angle, r is the distance between the measuring point and the centre of the sphere, ρ_1 is the resistivity of the medium, ρ_2 is the resistivity of the sphere and ρ_0 is the radius of the sphere. The scalar potential caused by a constant electric dipole is given by the formula(He, 2012)

$$U = \frac{I\mathrm{dl}}{4\pi\sigma}\cdot\frac{(-x)}{R^3} = -\mathrm{P}_0\frac{x}{R^3} \tag{7}$$

Where $\frac{x}{R} = cos\theta$. In equation (1.6) and (1.7), $R = r$, $P_0 = M$. So we get the potential distribution along the surface of a uniformly polarized sphere is equivalent to an electric dipole.

2.2 Two layers of medium

When there is a two-layer medium model, we discuss the air-sea water model and the sea-water-seafloor model. In the first model, we suppose the location of the image of the source $\mathbf{I}_x^{'}d\mathbf{l}$ is $(x_0, y_0, -z_0)$, when the measuring point is in the sea($z > 0$). It's assumed that the whole space is filled with seawater. We have the scalar potential of the source and the image:

$$\Phi_{sea}{=}\frac{I_x\mathrm{d}l(x-x_0)}{4\pi\sigma_1 R_1^3} + \frac{I_x^{'}\mathrm{d}l(x-x_0)}{4\pi\sigma_1 R_0^3}(z>0) \tag{8}$$

where $r_0 = (x-x_0)\mathbf{i} + (y-y_0)\mathbf{j} + (z+z_0)\mathbf{k}$, $r_1 = (x-x_0)\mathbf{i} + (y-y_0)\mathbf{j} + (z-z_0)\mathbf{k}$

If the measuring point is in the air($z \le 0$), the location of the image of the source is (x_0, y_0, z_0), which is coincided with the source. We suppose the whole space is filled with air. The combined dipole moment $\mathbf{I}_x^{"}d\mathbf{l}$ is

$$\Phi_{air} = \frac{I_x^{''}\mathrm{d}l(x-x_0)}{4\pi\varepsilon_0 R_1^3}(z\le 0) \tag{9}$$

where $r_1 = (x-x_0)\mathbf{i} + (y-y_0)\mathbf{j} + (z-z_0)\mathbf{k}$.

It can be obtained from the boundary conditions of the mirror image theory:

1) The potential of both sides of the surface is continuous($(\Phi_{sea}|_{z\to 0^+} = \Phi_{air}|_{z\to 0^-})$). We have:

$$\frac{I_x^{''}}{\varepsilon_0} = \frac{I_x^{'} + I_x}{\sigma_1} \tag{10}$$

https://doi.org/10.5194/gmd-2023-94
Preprint. Discussion started: 18 August 2023

Geoscientific Model Development Discussions

2) The current normal vectors on both sides of the interface are continuous and satisfy the boundary condition $j_{1z}|_{z\to 0^+} = j_{0z}|_{z\to 0^-}$. We have $\sigma_1 \frac{\partial \Phi_{sea}}{\partial z}\Big|_{z\to 0^+} = \sigma_0 \frac{\partial \Phi_{air}}{\partial z}\Big|_{z\to 0^-}$. Because in the air $\sigma_0 = 0$,only $\sigma_1 \frac{\partial \Phi_{sea}}{\partial z}\Big|_{z\to 0^+} = 0$ can satisfy the boundary condition,we have:

$$I_x^{'} = I_x \tag{11}$$

Using equations (10) and (11), we obtain

$$I_x^{''} = \frac{2\varepsilon_0}{\sigma_1} I_x \tag{12}$$

The above analysis shows the horizontal dipole has two situations when it is in the air-sea water model. If the measuring point is in the sea, the location of the mirror image $\mathbf{I}_x^{'}d\mathbf{l}$ is $(x_0, y_0, -z_0)$. If the measuring point is in the air, the mirror image coincides with the source (x_0, y_0, z_0) and the combined dipole is $\frac{2\varepsilon_0}{\sigma_1} I_x \mathrm{d}l$.

In the seawater-seafloor model, we can calculate like the first model. We suppose the electric dipole source $\mathbf{I}_x d\mathbf{l}$ is at (x_0, y_0, z_0). If we measure in the seawater, we can get the mirror image $\frac{\sigma_1-\sigma_2}{\sigma_1+\sigma_2}\mathbf{I}_x d\mathbf{l}$ is at $(x_0, y_0, -z_0)$. If the measuring point is on the seafloor, the mirror image is at (x_0, y_0, z_0) which the combined dipole is equivalent to $\frac{2\sigma_2}{\sigma_1+\sigma_2}\mathbf{I}_x d\mathbf{l}$. We supposed the measuring lines are in the seawater and compared the solution result of the sea water-seafloor model and the 2D analytical solution of the homogeneous half-space model. To verify the correctness of the mirror image method, we compare the 2D analytical solution inhomogeneous half-space and the analytical solution of the seawater-seafloor model. Based on the derivation above, the potential anomaly measured in the seawater of sea water-seafloor model can be expressed as:

$$\Phi = \frac{Ixdl(x-x_0)}{4\pi\sigma_1\left[(x-x_0)^2+(-z+z_0)^2\right]^{3/2}} + \frac{\frac{\sigma_1-\sigma_2}{\sigma_1+\sigma_2} Ixdl(x-x_0)}{4\pi\sigma_1\left[(x-x_0)^2+(z-z_0)^2\right]^{3/2}} \tag{13}$$

The 2D analytical solution in homogeneous half-space can be expressed as(Xie et al., 2021a):

$$U = M \cdot \frac{x\cos a - h_0 \sin a}{\left(h_0^2 + x^2\right)^{3/2}} \tag{14}$$

where $\mathbf{M}$ is the electric dipole moment, α is the polarizing angle and h_0 is the depth of the electric dipole. The comparison results and the error graph is shown in Fig.2. The error between the 2D analytical solution in homogeneous half-space and the analytical solution of the mirror image method is 0.0156‰. It proves the mirror image method is correct in calculating the polarization self-potential.

2.3 Three layers of medium

The actual ocean environment can be reduced to a three-layer model consisting of air, seawater and seafloor. The source "creates" countless mirror images among the three mediums. In the ocean model shown in Figure.3, the potential produced by an electric dipole in the seafloor can be equivalent to the superposition of the source and an infinite number of mirror images. We divide mirror images into four categories for their different locations and dipole moments.The locations and potentials of these mirror images are shown in the table 1.

https://doi.org/10.5194/gmd-2023-94
Preprint. Discussion started: 18 August 2023

Geoscientific Model Development Discussions

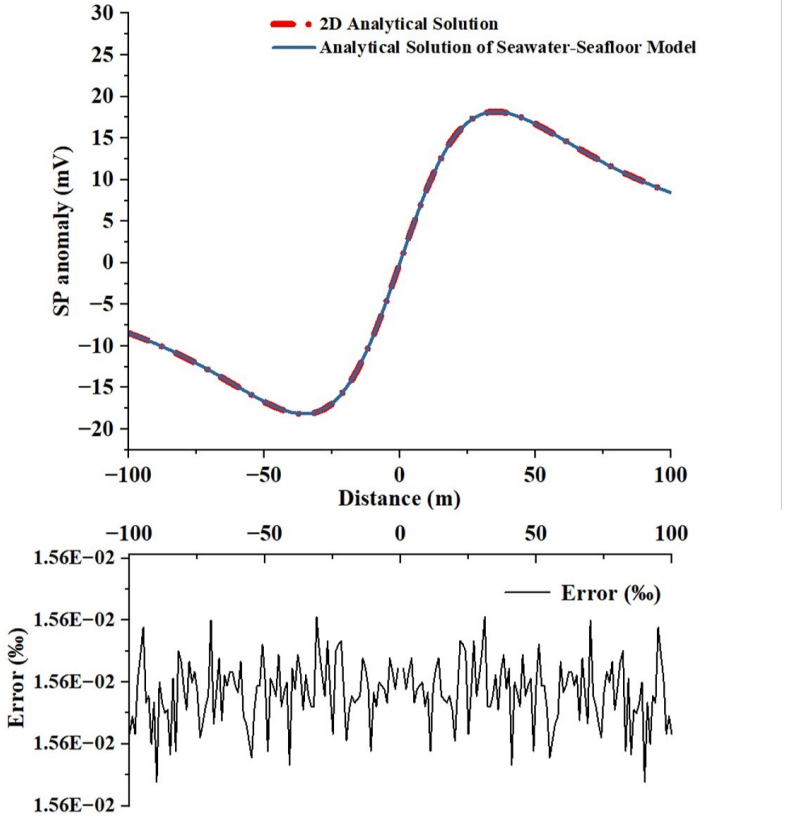

Figure 2. The comparison of the analytical solution of the seawater-seafloor model. The analytical solution of the mirror image method is consistent with the 2D analytical solution.

Table 1. Locations and dipole moments of the source and mirror images

	location	*Dipole moments*	*The position vector between the measuring point and the source*
1	$(x_0, y_0, 2\mathrm{m}D - z_0)$	$\left(\frac{\sigma_1-\sigma_2}{\sigma_1+\sigma_2}\right)^{\mathrm{m}} \mathbf{I}_x d\mathbf{l} = \eta^m \mathbf{I}_x d\mathbf{l} \mathbf{i} (m = 1, 2, ...)$	$\mathbf{r}_{1m} = (x-x_0)\mathbf{i}+(y-y_0)\mathbf{j}+(z-2mD+z_0)\mathbf{k}$
2	$(x_0, y_0, 2\mathrm{m}D + z_0)$	$\left(\frac{\sigma_1-\sigma_2}{\sigma_1+\sigma_2}\right)^{\mathrm{m}} \mathbf{I}_x d\mathbf{l} = \eta^m \mathbf{I}_x d\mathbf{l} \mathbf{i} (m = 1, 2, ...)$	$\mathbf{r}_{2m} = (x-x_0)\mathbf{i}+(y-y_0)\mathbf{j}+(z-2mD-z_0)\mathbf{k}$
3	$(x_0, y_0, -2\mathrm{n}D + z_0)$	$\left(\frac{\sigma_1-\sigma_2}{\sigma_1+\sigma_2}\right)^{\mathrm{n}} \mathbf{I}_x d\mathbf{l} = \eta^n \mathbf{I}_x d\mathbf{l} \mathbf{i} (n = 0, 1, ...)$	$\mathbf{r}_{1\mathrm{n}} = (x-x_0)\mathbf{i}+(y-y_0)\mathbf{j}+(z+2nD-z_0)\mathbf{k}$
4	$(x_0, y_0, -2\mathrm{n}D - z_0)$	$\left(\frac{\sigma_1-\sigma_2}{\sigma_1+\sigma_2}\right)^{\mathrm{n}} \mathbf{I}_x d\mathbf{l} = \eta^n \mathbf{I}_x d\mathbf{l} \mathbf{i} (n = 0, 1, ...)$	$\mathbf{r}_{2\mathrm{n}} = (x-x_0)\mathbf{i}+(y-y_0)\mathbf{j}+(z+2nD+z_0)\mathbf{k}$

https://doi.org/10.5194/gmd-2023-94
Preprint. Discussion started: 18 August 2023

Geoscientific Model Development Discussions

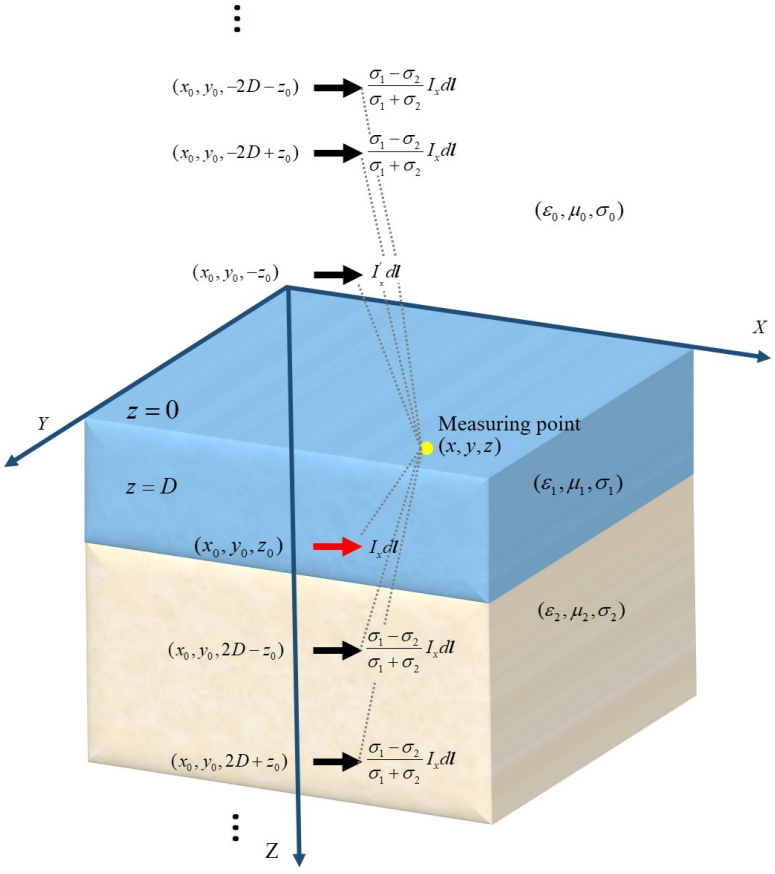

Figure 3. Sketch of three layers of medium in SMS model. The yellow point represents the measuring point, the red arrow represents the electric dipole and the black arrows represent mirror images of the source.

The scalar potential of the horizontal electric dipole $P_x = \mathbf{I}_x d\mathbf{l}i$ at the measuring point for any dipole moment in the seafloor can be expressed as

$$\Phi_x(x,y,z) = \sum_{m=1}^{\infty} \left[\frac{\eta^m I_x dl(x-x_0)}{4\pi\sigma_1 r_{1m}^3} + \frac{\eta^m I_x dl(x-x_0)}{4\pi\sigma_1 r_{2m}^3} \right] + \sum_{n=0}^{\infty} \left[\frac{\eta^n I_x dl(x-x_0)}{4\pi\sigma_1 r_{1n}^3} + \frac{\eta^n I_x dl(x-x_0)}{4\pi\sigma_1 r_{2n}^3} \right] \tag{15}$$

The expression of r_{1m}, r_{2m}, r_{1n}, and r_{2n} is shown in table 1. The electric dipoles in the other two directions $P_y = \mathbf{I}_y d\mathbf{l}j$ and
130 $P_z = \mathbf{I}_z d\mathbf{l}k$ can be expressed by the same method. So we can get the potential of the electric dipole $P = \mathbf{I}_x d\mathbf{l}i + \mathbf{I}_y d\mathbf{l}j + \mathbf{I}_z d\mathbf{l}k$

https://doi.org/10.5194/gmd-2023-94
Preprint. Discussion started: 18 August 2023

Geoscientific Model Development Discussions

in any direction which can be equivalent to the superposition of the source and the countless mirror images:

$$\Phi(x,\mathrm{y},z)=\Phi_x(x,\mathrm{y},z)+\Phi_y(x,\mathrm{y},z)+\Phi_z(x,\mathrm{y},z)=$$
$$\sum_{m=1}^{\infty}\left[\begin{array}{l}\frac{\eta^m I_x dl(x-x_0)}{4\pi\sigma_1 r_{1m}^3}+\frac{\eta^m I_y dl(y-y_0)}{4\pi\sigma_1 r_{1m}^3}-\frac{\eta^m I_z dl(z-2mD+z_0)}{4\pi\sigma_1 r_{1m}^3}\\ +\frac{\eta^m I_x dl(x-x_0)}{4\pi\sigma_1 r_{2m}^3}+\frac{\eta^m I_y dl(x-x_0)}{4\pi\sigma_1 r_{2m}^3}+\frac{\eta^m I_z dl(z-2mD-z_0)}{4\pi\sigma_1 r_{2m}^3}\end{array}\right]+$$
$$\sum_{n=0}^{\infty}\left[\begin{array}{l}\frac{\eta^m I_x dl(x-x_0)}{4\pi\sigma_1 r_{1n}^3}+\frac{\eta^n I_y dl(y-y_0)}{4\pi\sigma_1 r_{1n}^3}+\frac{\eta^n I_z dl(z+2mD-z_0)}{4\pi\sigma_1 r_{1n}^3}\\ +\frac{\eta^n I_x dl(x-x_0)}{4\pi\sigma_1 r_{2n}^3}+\frac{\eta^n I_y dl(y-y_0)}{4\pi\sigma_1 r_{2n}^3}-\frac{\eta^n I_z dl(z+2mD+z_0)}{4\pi\sigma_1 r_{2n}^3}\end{array}\right] \quad (16)$$

3 Numerical calculation of electric dipole potential distribution in SMS

We carry out the numerical calculation of the electric potential distribution of the dipole in any direction. We suppose the seawater depth is 100 m and the seafloor extends indefinitely along the Z axis. The electric dipole simplified by spherical SMS is at the seafloor surface with location (0,0,100). The conductivity of the seawater (σ_1) and the seafloor (σ_2) is 4 S/m and 0.04 S/m and the dipole moment is 1 **D**. In the infinite summarization, the computation will end if the difference between the adjacent terms is less than 10-10. We calculated the potential distribution of a horizontal dipole along the Y-axis, a vertical dipole along the Z-axis and a tilted dipole as shown in figure.4. The result suggests the horizontal electric dipole reduces a positive SP anomaly and a negative SP anomaly on either of it. The absolute values of the exceptions are equal. There is a positive anomaly caused by a vertical electric dipole. The tilted electric dipole produces a positive and a negative SP anomaly like the horizontal electric dipole. But the absolute values of them are unequal because of the depth difference.

4 A experimental verification about 3D analytical solution of mirror image method

We built a system for self-potential measurements from a laboratory perspective (shown in fig.5) to prove the analytical solution. We built a flume, with a scale of 50cm×50cm×100cm, filled with sand and saline water to simulate the ocean environment. A sphere made of copper and iron was placed between the sand and the saline water (one half of the sphere is copper and the other half is iron). The redox reactions occurred on the surface of the sphere with the electronic transfer. So we can control the direction of the electric dipole by changing the polarization angle of the sphere. We measured the SP signal when the Cu-Fe interface and the XOY plane were at an angle of 0° and 45° to simulate a vertical and a tilted electric dipole. SP signal results shown in Fig.6 suggest the experimental result is in good agreement with the numerical solutions. The reduction reaction happened in the iron hemisphere which generated a negative SP value on the iron side. Similarly, a positive SP value appeared on the other side. Because the iron hemisphere was higher than the copper hemisphere, the absolute value of the negative SP value was greater than the positive SP value. To verify the validity of the 3D analytical solution, we compared the middle line of the measured data and the 3D analytical solution. The result is also shown in Fig.6. From these results, the 3D measured data plane is in good agreement with the 3D analytical solution.

https://doi.org/10.5194/gmd-2023-94
Preprint. Discussion started: 18 August 2023

Geoscientific Model Development
Discussions
Open Access
EGU

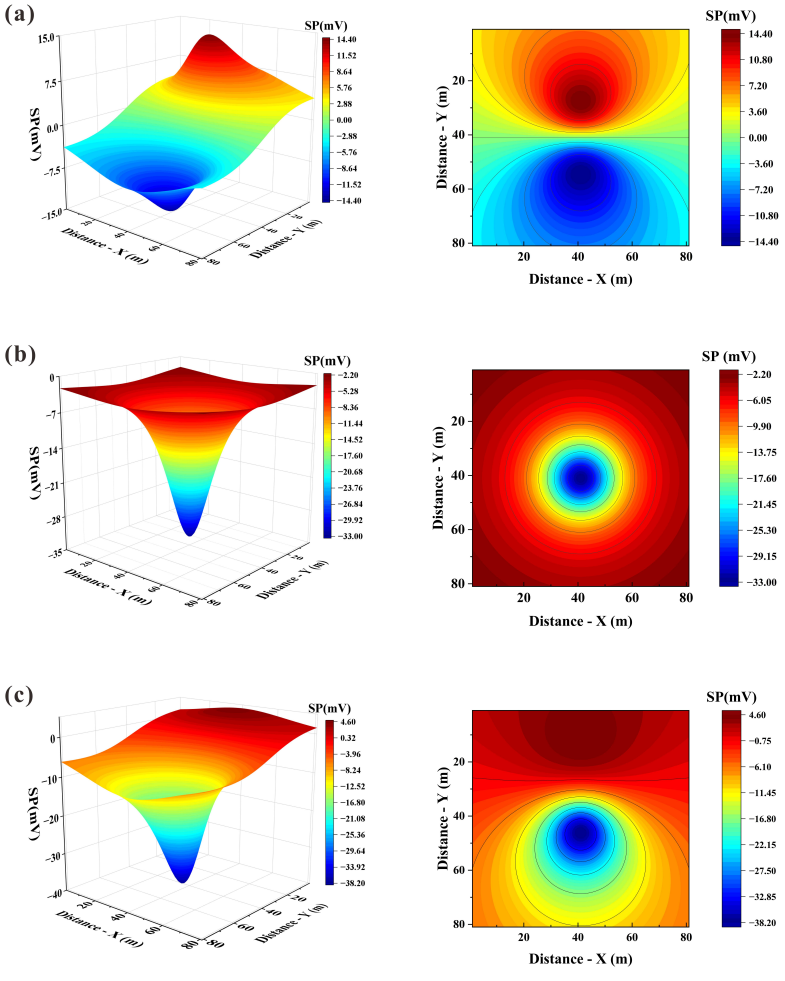

Figure 4. Analytical solution result and contour map of the different dipole. **a** horizontal electric dipole; **b** vertical electric dipole; **c** tilted electric dipole with an angle of 45° from the XOY plane.

https://doi.org/10.5194/gmd-2023-94
Preprint. Discussion started: 18 August 2023

Geoscientific Model Development Discussions
Open Access
EGU

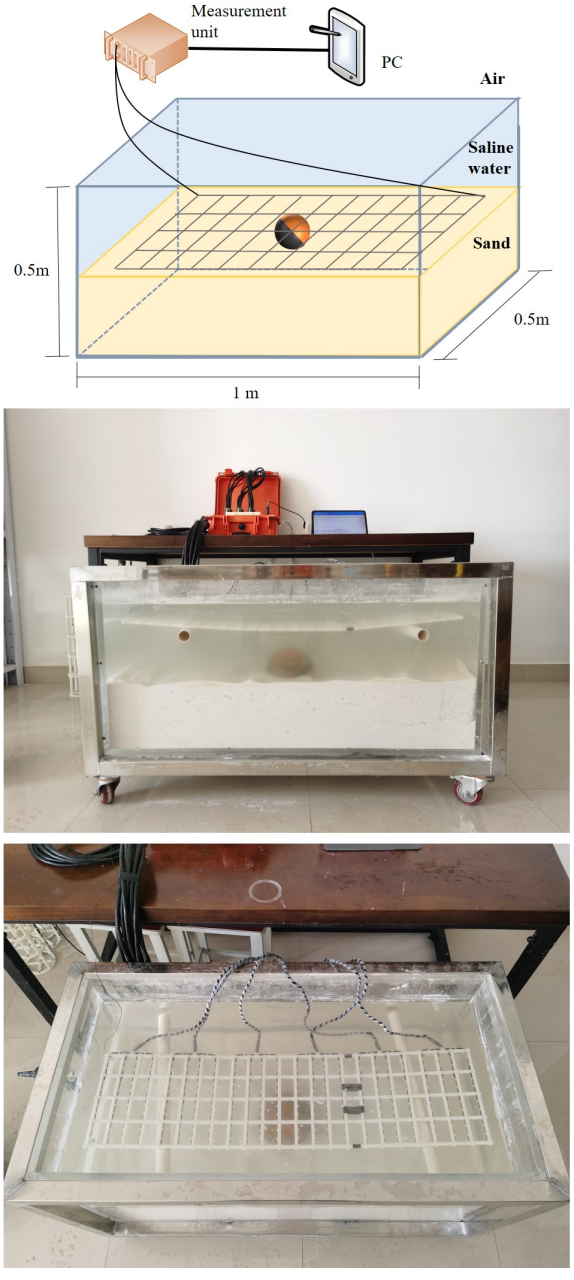

Figure 5. Sketch of SP measuring system. A Fe-Cu sphere was placed in the interface of saline water and the sand. According to the time-lapse data, the redox process was stable after 20 hours. We used the stabilized polarization data for analysis.

https://doi.org/10.5194/gmd-2023-94
Preprint. Discussion started: 18 August 2023

Geoscientific Model Development
Discussions
Open Access
EGU

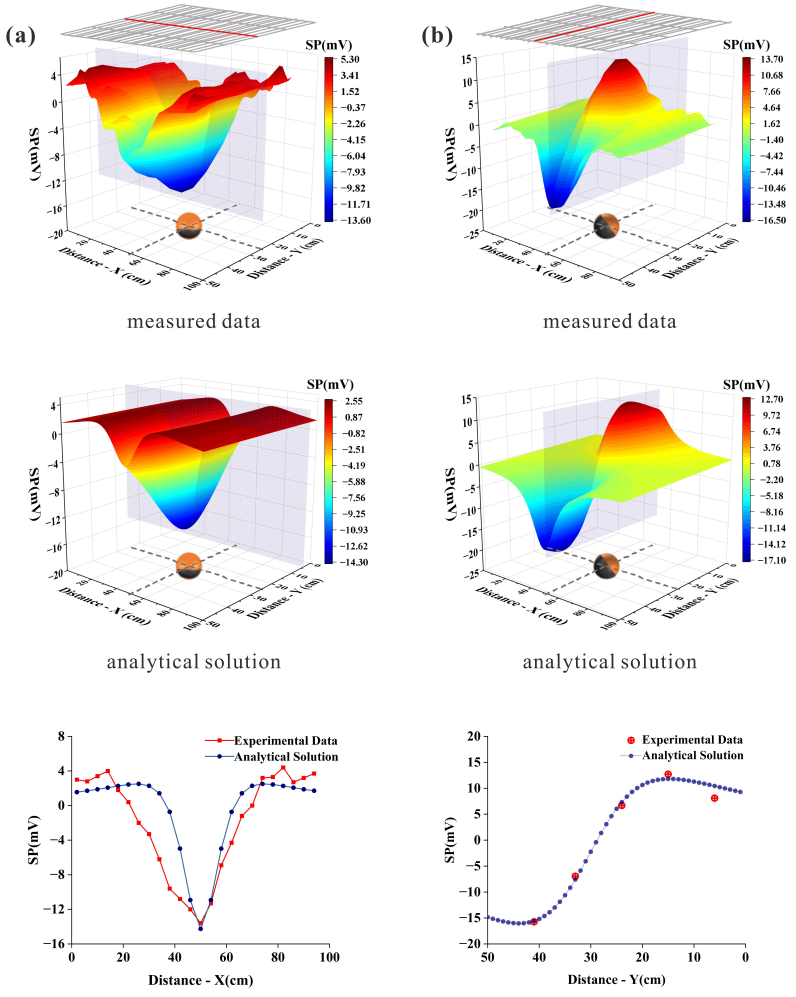

Figure 6. Results of SP signals and comparison of the measuring data and analytical solution. **a** vertical electric dipole; **b** tilted electric dipole; The gray frame represents the measurement system, and the red line is the middle measurement line.

https://doi.org/10.5194/gmd-2023-94
Preprint. Discussion started: 18 August 2023


Geoscientific Model Development Discussions

5 Conclusions

The 3D SP analytical solution from regularly polarized bodies in a layered seafloor model plays a key role in mineral exploitation and forward modeling of the SP method. So we used the mirror image method to calculate the 3D spatial analytical solution. Based on a discussion about the equivalent relationship between a sphere and electric dipole, we derived the formula of two-layer and three-layer models consist of different mediums by superposition of the scalar field generated by the source and mirror images in different mediums. The correctness of the mirror image method is proved by the comparison of the 2-layer model and the analytical solution in homogeneous half-space. To prove the validity of the 3D analytical solution further, we took an experiment which is built to simulate a simplified SMS model. By changing the angle of a Fe-Cu sphere interface and XOY plane, we discuss different electric field distributions and compared the results of the middle line with the 2D analytical solutions. The results show that analytical solution based on the mirror image method is effective for forward modeling in SMS exploration.

Code availability. The code are written in Matlab and figures are displayed with Origin software.
The code and the data is available at: https://doi.org/10.5281/zenodo.8082740

Data availability. The source data is available at: https://doi.org/10.5281/zenodo.8082740

Author contributions. Pengfei Zhang is the first author of this paper. It's part of his research project. He conceived, designed the study, conducted the experiment and wrote the paper. Yi-an Cui designed the study and experiment. Jing Xie and Youjun Guo developed the idea for the study and did some analyses about the data. Jieran Liu collected the experiment data. All authors discussed the results and revised the manuscript.

Competing interests. The contact author has declared that none of the authors has any competing interests

Acknowledgements. This work was financially supported by the National Natural Science Foundation of China (42174170, 41874145, 72088101).

https://doi.org/10.5194/gmd-2023-94
Preprint. Discussion started: 18 August 2023

References

Alarouj, M. and Jackson, M. D.: Numerical modeling of self-potential in heterogeneous reservoirs, Geophysics, 87, E103–E120, 2022.

Bérubé, A. P.: A Graphical 3D Finite Element Program for Modelling Self-Potentials Generated by Flow Through a Porous MediumA Graphical 3D FEM Program for Modelling SP, Journal of Environmental and Engineering Geophysics, 12, 185–197, 2007.

Bhattacharya, B. and Roy, N.: A note on the use of a nomogram for self-potential anomalies, Geophysical Prospecting, 29, 102–107, 1981.

Biswas, A. and Sharma, S. P.: Resolution of multiple sheet-type structures in self-potential measurement, Journal of Earth System Science, 123, 809–825, 2014.

Constable, S., Kowalczyk, P., and Bloomer, S.: Measuring marine self-potential using an autonomous underwater vehicle, Geophysical Journal International, 215, 49–60, 2018.

Corliss, J. B., Dymond, J., Gordon, L. I., Edmond, J. M., von Herzen, R. P., Ballard, R. D., Green, K., Williams, D., Bainbridge, A., Crane, K., et al.: Submarine thermal springs on the Galapagos Rift, Science, 203, 1073–1083, 1979.

Corwin, R.: Offshore use of the self-potential method, Geophysical Prospecting, 24, 79–90, 1976.

Dmitriev, A.: Forward and inverse self-potential modeling: a new approach1, Russian Geology and Geophysics, 53, 611–622, 2012.

El-Araby, H. M.: A new method for complete quantitative interpretation of self-potential anomalies, Journal of applied Geophysics, 55, 211–224, 2004.

Fornasari, G., Capozzoli, L., and Rizzo, E.: Combined GPR and Self-Potential Techniques for Monitoring Steel Rebar Corrosion in Reinforced Concrete Structures: A Laboratory Study, 15, 2206, https://www.mdpi.com/2072-4292/15/8/2206, number: 8 Publisher: Multidisciplinary Digital Publishing Institute.

Guo, Y., Cui, Y.-a., Xie, J., Luo, Y., Zhang, P., Liu, H., and Liu, J.: Seepage detection in earth-filled dam from self-potential and electrical resistivity tomography, Engineering Geology, 306, 106 750, 2022.

Hannington, M., Jamieson, J., Monecke, T., Petersen, S., and Beaulieu, S.: The abundance of seafloor massive sulfide deposits, Geology, 39, 1155–1158, 2011.

He, J.: Principles of Marine electromagnetic method, Beijing:Higher Education Press, 2012.

Kawada, Y. and Kasaya, T.: Marine self-potential survey for exploring seafloor hydrothermal ore deposits, Scientific reports, 7, 1–12, 2017.

Li, J. et al.: Geoelectric field and electrical exploration, Beijing: Geological Publishing House, 2005.

Mendonca, C. A.: Forward and inverse self-potential modeling in mineral exploration, Geophysics, 73, F33–F43, 2008.

Safipour, R., Hölz, S., Halbach, J., Jegen, M., Petersen, S., and Swidinsky, A.: A self-potential investigation of submarine massive sulfides: Palinuro Seamount, Tyrrhenian Sea, Geophysics, 82, A51–A56, 2017.

Satyanarayana Murty, B. and Haricharan, P.: Nomogram for the complete interpretation of spontaneous potential profiles over sheet-like and cylindrical two-dimensional sources, Geophysics, 50, 1127–1135, 1985.

Sheffer, M. and Oldenburg, D.: Three-dimensional modelling of streaming potential, Geophysical Journal International, 169, 839–848, 2007.

Stephenson, U.: Comparison of the mirror image source method and the sound particle simulation method, Applied Acoustics, 29, 35–72, 1990.

Su, Z., Tao, C., Shen, J., Revil, A., Zhu, Z., Deng, X., Nie, Z., Li, Q., Liu, L., Wu, T., et al.: 3D self-potential tomography of seafloor massive sulfide deposits using an autonomous underwater vehicle, Geophysics, 87, B255–B267, 2022.

Wang, P., Chen, X., Li, J., and Wang, B.: Accurate porosity prediction for tight sandstone reservoir: A case study from North China, Geophysics, 85, 1–71, 2019.

https://doi.org/10.5194/gmd-2023-94
Preprint. Discussion started: 18 August 2023

Wei, K., Chen, B., and Peng, J.: G&M3D 1.0: an Interactive framework for 3D Model Construction and Forward Calculation of Potential Fields, Geoscientific Model Development Discussions, 2023, 1–20, 2023.

Xie, J., Cui, Y.-a., Guo, Y., Zhang, L., Fanidi, M., and Liu, J.: 2.5 D self-potential forward modeling by natural-infinite element coupling method, Journal of Applied Geophysics, 179, 104 077, 2020a.

Xie, J., Cui, Y.-a., Zhang, L., Guo, Y., Wang, J., Fanidi, M., and Liu, J.: Numerical modeling of biogeobattery system from microbial degradation of underground organic contaminant, SN Applied Sciences, 2, 1–11, 2020b.

Xie, J., Cui, Y.-a., Zhang, L., Ma, C., Yang, B., Chen, X., and Liu, J.: 3D forward modeling of seepage self-potential using finite-infinite element coupling method, Journal of Environmental and Engineering Geophysics, 25, 381–390, 2020c.

Xie, J., Cui, Y. A., Fanidi, M., Zhang, L., Guo, Y., Luo, Y., and Liu, J.: Numerical Modeling of Marine Self-Potential from a Seafloor Hydrothermal Ore Deposit, Pure and Applied Geophysics, 178, 1731–1744, 2021a.

Xie, J., Cui, Y.-a., Fanidi, M., Zhang, L., Guo, Y., Luo, Y., and Liu, J.: Numerical modeling of marine self-potential from a seafloor hydrothermal ore deposit, Pure and Applied Geophysics, 178, 1731–1744, 2021b.

Yungul, S. H.: Interpretation of spontaneous polarization anomalies caused by spheroidal ore bodies, Geophysics, 15, 237–246, 1950.